Organic Process Research & Development

ARTICLE

pubs.acs.org/OPRD

Impact of Laboratory Vacuum Contact Drying on Material Drying Rates and Physical Properties

P. Kontcho Kom, W. Cook, and E. Kougoulos*

Pfizer Pharmatherapeutics, Ramsgate Road, Sandwich, Kent CT13 9NJ, U.K.

ABSTRACT: In this study, the effect of different laboratory vacuum contact drying methods on the drying rates and physical properties of Lactose FastFlo 316, Avicel PH200, and an active pharmaceutical ingredient (API) were investigated. The influence of various types of dryers (conical screw, tray, and rotary drying on the drying) performance of Lactose FastFlo 316 was investigated. Conical screw drying was found to produce the best drying performance, but considerable attrition and agglomeration was observed. Tray drying was found to have the poorest drying performance with the greatest degree of particle agglomeration being observed when compared to rotary and conical screw drying. The impact of the various types of dryers on the particle size and size distribution of Avicel PH200 was found to be minimal when compared to the reference. For rotary drying, the effects of drying temperature, initial moisture content, median particle size input, vacuum pressure, and rotary speed on the drying rate and particle size distribution was assessed using the API. An increase in median particle size and rotary speed with a reduction in moisture content and vacuum pressure resulted in a decrease in overall drying times. An increase in rotary speed was found to decrease the particle size for both small and large input particle sizes as a result of attrition. In addition, to the drying equipment and conditions, the material properties are also important in determining whether attrition and/or agglomeration events will occur.

1. INTRODUCTION

Drying is the last active step following crystallization and filtration[1,2] in the primary manufacture of active pharmaceutical ingredients (APIs). Particle engineering through crystallization is a process that allows both the physical and chemical properties of the API to be controlled.[3] However, the impact of drying processes postcrystallization on the powder properties is poorly understood, and currently no tools are available to predict behaviour and scale-up performance. Contact drying involves transfer of heat to wet material mainly by conduction from a hot surface. Many APIs and excipients are heat sensitive and require temperature control to avoid degradation. Contact dryers are very popular in the pharmaceutical industry because of their closed design and their ability to operate under vacuum. Working under reduced pressures allows drying at lower temperatures and therefore is suitable for handling such temperature-sensitive materials. Vacuum enhances the drying rate by lowering the absolute pressure of the system below the vapour pressure of the solvent.[4] Multiscale modelling with experimental validation of heat transfer to include effects of temperature, pressure, and moisture content has been carried out on contact dryers[5−8] including the effects of heat transfer in indirect heat-agitated dryers.[9] Furthermore, modelling heat transfer and the effects of temperature and residual solvent moisture content on drying kinetics for various materials has also been studied in tray dryers,[10] rotary dryers,[11,12] and agitated dryers.[13,14] Process analytical techniques (PAT) to include near infrared (NIR) spectroscopy has also recently found application in monitoring residual solvent moisture content in contact dryers.[15] Drying is often accompanied by changes in the physical properties of the solid, as undesirable phenomena such as agglomeration and attrition can occur. However, little literature is available on this subject. Attrition can lead to the formation of very small particles causing, for example, poor flowability of the product. On the other hand, agglomeration may cause the formation of large particles that may reduce the dissolution rate of the drug. Lekhal et al.[16,17] have recently studied the impact of crystal habit on the drying kinetics in agitated filter dryers. During the study of the impact of agitated drying on crystal morphology of potassium chloride, Lekhal et al. found that attrition was caused by particle−particle collisions, particle-wall collisions as well as shear due to the rotation of the impeller.

This paper focuses on assessing the heat transfer performance and impact on physical properties of three laboratory contact dryers namely: tray, rotary, and conical screw dryers using lactose monohydrate (FastFlo 316) and microcrystalline cellulose (Avicel PH200) as model compounds. With lactose monohydrate the drying kinetics were investigated with overall heat transfer coefficients being estimated for these laboratory dryers. With microcrystalline cellulose and lactose monohydrate, the impact of the various laboratory dryers on the physical properties from an agglomeration and attrition perspective was investigated. The impact of input particle size and effect of rotary drying (vacuum pressure, drying temperature, rotary speed) using the active pharmaceutical ingredient (API) on the final API particle size and size distribution was investigated.

2. THEORY

Heat transferred from the heated surface to the bed is used not only to heat the wet material but also to evaporate the solvent

Received: October 18, 2010
Published: February 08, 2011

dx.doi.org/10.1021/op1002787 | *Org. Process Res. Dev.* 2011, 15, 360–366

contained in the bed. Therefore, a general formula for the heat transferred to the bed can be written as follows:

$$Q_{bed} = Q_m + Q_{ev} = UA(T_m - T_b) \quad (1)$$

The overall heat transfer coefficient U takes into account all the individual heat transfer coefficients as well as resistances. It is calculated as the reciprocal sum of thermal resistances. It is used for performance assessment of dryers because it is a characteristic of the amount of heat conveyed to the wet material. The overall heat transfer coefficient (U) for contact drying was estimated as follows:

$$U = \frac{1}{\frac{1}{h_{medium\text{-}walls}} + \frac{x_w}{\lambda_G} + \frac{1}{h_{walls\text{-}particles}} + \frac{x_f}{\lambda_V}} \quad (2)$$

1. The first term represents the heat transfer from the heating medium to the outer walls. It takes place by convection and depends on the heat transfer coefficient of the utility used.
2. The second term denotes the heat transfer through the walls. It takes place by conduction and is calculated as the ratio of the wall thickness and the conductivity of the wall. The thicker the wall, the more resistant it is to heat transfer.
3. The third term represents the heat transfer coefficient from the inner walls to the first layer of particles. It was calculated as a function of drying rate (dW_t/dt).

$$h_{wall\text{-}particles} = \frac{dW_t\beta}{dtA(T_m - T_b)} \quad (3)$$

where β is the latent heat of evaporation of the solvent.

4. The fourth term represents the heat transfer coefficient from the first layer of particles to the bulk which was estimated as the ratio of the thickness of film formed near the walls and film wall conductivity.

3. EXPERIMENTAL SECTION

3.1. Materials. Lactose FastFlo 316 and Avicel PH200 were obtained from Foremost Farms, Wisconsin, U.S.A. and FMC Biopolymer, respectively. The API was manufactured by crystallization from acetone and water using a reverse antisolvent crystallization method at ambient temperature. Acetone with HPLC purity >99.9% was purchased from Sigma-Aldrich, and deionized water was used for the crystallization experiments. The active pharmaceutical ingredient (API), lactose, and Avicel have a needle, tomahawk, and irregular crystal habit, respectively.

3.2. Material Characterisation. *Particle Size Distribution.* A Sympatec HELOS system was used to measure particle size distribution for Avicel PH200 and Lactose FastFlo 316. An R5 lens was used with a size range of 4.5−1750 μm. A VIBRI feeder was used with an OASISDRY 4 mm disperser at 3.0 bar pressure used for dispersion. Measurements were made in triplicate. A Malvern Mastersizer 2000 instrument using a wet dispersion method was used to measure the particle size distribution of the API. Measurements were made in triplicate.

3.3. Equipment. *Rotary Dryer.* A laboratory-scale Buchi rotary evaporator was used for rotary drying experiments. A Buchi Vacuum V-800 controller was used to control the vacuum level (±0.05 kPa). A Buchi R-205 rotavaporator system was used to control the rotation speed of a 1-L round-bottomed glass flask with an operating range between 0 and 250 rpm. A Buchi B-490 water heating bath with temperature control was used (±2.5 °C). The cake temperature was recorded as a function of time using an infrared thermometer gun (control company model FB70328, with a temperature range of 50−1000 °C and a resolution of 0.1 °C). The moisture content was recorded by taking subsamples (approximately 0.25 g) of the cake by breaking vacuum and determining the loss on drying (LOD) using a Sartorius Moisture Analyzer (model MA150) until a steady state measurement was achieved.

Tray Dryer. A digital Solvis Lab Vacucenter dryer (model VC50) was used for all vacuum tray drying experiments. A 1-L flat-bottomed glass dish was used for loading wet cake for all drying experiments. The cake temperature and the LOD were measured using the analytical equipment described above.

Conical Screw Dryer. A 1-L Bolz-Summix mini-dry system from Bolz-Summix was used for all conical screw drying experiments. The equipment consisted of a conical feed vessel equipped with an external drive unit and an internal mixing screw guided by an orbital arm. The drying heat was supplied via the conical double jacketed walls as well as the heated screw. The closed system allowed working under vacuum. Pressure and temperature sensors enabled monitoring of process parameters such as vacuum pressure, cake temperature, and jacket temperature. Subsamples were taken for LOD measurements at different time intervals.

Table 1. Process conditions used for rotary drying experiments used for the API

experiment	median particle size input $D[_{0.5}]$ [μm]	initial moisture content [% w/w]	drying temperature [°C]	vacuum level [kPa]	rotary speed [rpm]
1	5	43	50	2	50
2	5	46	70	2	50
3	40	24	50	2	50
4	40	25	70	2	50
5	5	44	50	2	10
6	5	43	50	2	240
7	40	19	50	2	10
8	40	22	50	2	240
9	5	41	50	50	50
10	40	16	50	50	50

3.4. Experimental Conditions. Both small and large particles of the API were manufactured to feed into rotary drying experimentation by varying the crystallization conditions. A solution of API dissolved in acetone was added to aqueous solutions of varying compositions ranging from neat water to mixtures of water and acetone to manipulate particle size. The cakes were washed with water.

The small particles had a median size (D [v, 0.5]) of 5 μm, whereas the large particles had a median size of 40 μm. A 1-L LabMax automated process reactor (from Mettler-Toledo) with overhead agitation was used to manufacture bulk material. The particles produced from the crystallization were isolated using vacuum filtration, and the initial moisture content postfiltration and washing was recorded. For the drying experiments using Avicel PH200 and Lactose FastFlo 316, deionized water was added to the dry powder to provide the initial moisture content. Table 1 shows the process conditions used for the rotary drying experiments for the API. All experiments were carried out on a

dx.doi.org/10.1021/op1002787 |Org. Process Res. Dev. 2011, 15, 360–366

Table 2. Drying equipment and process conditions used for Lactose FastFlo 316 and Avicel PH200

drying equipment	scale [g]	initial moisture content [% w/w]	drying temperature [°C]	vacuum level [kPa]	speed [rpm]	arm speed [rpm]
rotary dryer	100	16	50	2	190	n/a
conical screw dryer	100	16	50	2	190	2
tray dryer	100	16	50	2	n/a	n/a

Table 3. Process parameters for various dryer used to estimate overall heat transfer coefficients

process parameters	rotary	tray	conical screw
latent heat vaporisation of water [J kg^{-1}]	2257000	2257000	2257000
heat transfer area [m^2]	0.00565	0.0077	0.0075
convective heat transfer coefficient heating medium-wall [W m^{-2} K^{-1}]	1000	2000	2000
wall thickness [m]	0.001	0.001	0.01
thermal conductivity [W m^{-1} K^{-1}]	0.78	0.78	18
film thickness at wall [m]	0.0015	0.0015	0.0015
film wall conductivity [W m^{-1} K^{-1}]	0.2	0.2	0.2

30-g scale. The initial moisture content post vacuum filtration for the particles with a median size of 5 and 40 μm ranged between 41 and 46% w/w and 16−25% w/w, respectively. The values were selected to investigate high and low values of each process parameter. A fractional experimental design was not considered.

Table 2 shows the drying equipment and process conditions used for Lactose FastFlo 316 and Avicel PH200.

Table 3 shows process data that was used for estimating overall heat transfer coefficients for the various dryers used for Lactose FastFlo 316.

4. RESULTS AND DISCUSSION

Case Study 1: Lactose FastFlo 316 Drying Kinetics. Table 2 shows the drying and process conditions used for Lactose FastFlo 316 drying experiments. Figure 1 shows the evolution of cake temperature, cumulative LOD, drying rate, and estimated overall heat transfer coefficients as a function of drying time for Lactose FastFlo 316 on a 100-g scale and drying at 50 °C and 2 kPa respectively.

Figure 1a shows an increase in cake temperature as the drying progresses, corresponding to an increase in the LOD (Figure 1b). As the moisture content decreased, the vacuum level in the system also increased. Hence, cake temperature measurement is a simple and effective method of monitoring drying progression without the need to use expensive PAT methods such as mass spectroscopy and NIR spectroscopy,[15] although the latter offers distinct advantages when multiple solvent systems are present. The tray dryer exhibited the slowest increase in cake temperature and LOD followed by the rotary dryer and conical screw dryer, respectively; overall, however, the LOD curve for the tray dryer is not as sharp as expected. Potentially, positioning of the temperature probe could be important. With the exception of the conical screw dryer, two distinct zones can be determined in the dying rate curves (Figure 1c). The first zone where the drying rate increases and which is considered the preheating period on a typical drying curve and a second zone known as the falling rate period where the drying rate falls and asymptotically approaches zero when the bed moisture content approaches the equilibrium moisture content. No pseudoconstant period was observed with any of the drying experiments. As far as the drying curve for the conical screw dryer was concerned, preheating and pseudoconstant rate periods were not observed probably because these periods were too short due to the fast drying rate and the technique used for LOD recording, which did not allow the drying cake mass to be recorded at short time intervals. From Figure 1c, the highest overall drying rates were achieved with the conical screw dryer and are almost 10 times greater compared to those with tray drying, the reasons being the effective three-dimensional mixing of the material by the screw which maximised surface renewal, and the efficient heat transfer provided by the heated jacketed wall of the equipment. The drying time achieved using the rotary dryer was about 15000 s (250 min), with maximum drying rate of 0.0005 kg solvent s^{-1} kg dry $solid^{-1}$, which is half of that of the conical screw dryer. Tray drying exhibited the poorest drying performance, with a drying time in excess of 21000 s (350 min). Figure 1d shows the overall heat transfer coefficients estimated for the three laboratory-scale dryers as a function of time. In most drying cases the constant-rate drying period is used to estimate heat transfer coefficients, but in our example there was no constant-rate drying period; hence, the entire experimental data set was used to estimate the overall heat transfer coefficient at each time interval. Equations 1, and 3 and process data defined in Table 3 were used to estimate overall heat transfer coefficients. Heat transfer coefficients express the ease of heat transfer to solids and are used to evaluate a dryers' performance. The values for heat transfer coefficient from the medium to the wall and that through the walls were found to be negligible but were included in the calculations for completeness. The dominant factor was heat transfer from the inner walls of the dryer to the first layer of the particles. As this was calculated from drying rates, it was found to decrease linearly with the moisture content. The overall heat transfer coefficients for all dryers were higher at the beginning of the drying process and decreased as drying progressed. This decrease was due to an increase in thermal resistance of the bed as it was drying. In other words, dry particles have higher thermal resistance than wet particles. As expected, the highest overall heat transfer coefficients were obtained with the laboratory conical screw dryer and varied between 25 and 95 W m^{-2} K^{-1}. Lower values were obtained in rotary and tray dryers, 0.5−19 W m^{-2} K^{-1} and 0.5−11 W m^{-2} K^{-1}, respectively. For tray drying this compares well with the literature value[19] of 5−6 W m^{-2} K^{-1}. For the rotary dryer, the experimental value is slightly lower than the literature value of 28−284 W m^{-2} K^{-1}.

dx.doi.org/10.1021/op1002787 |Org. Process Res. Dev. 2011, 15, 360–366

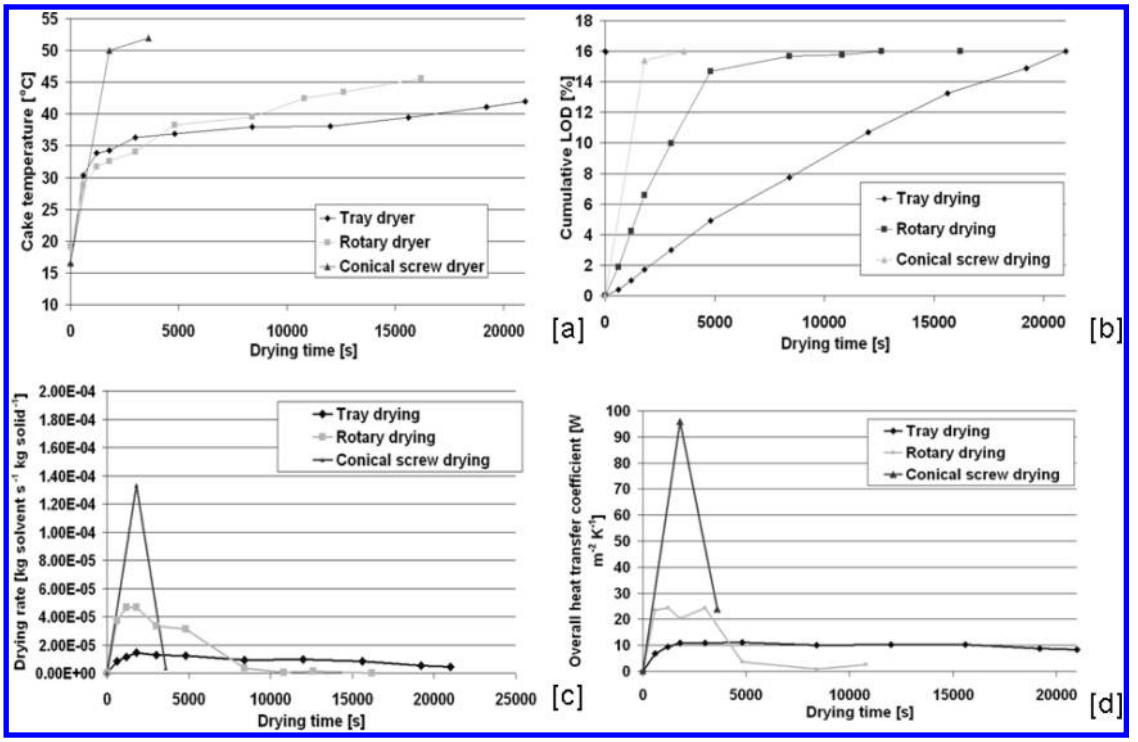

Figure 1. Lactose FastFlo 316 drying process data from various laboratory contact drying equipment. [a] Cake temperatures. [b] Cumulative loss on drying (LOD). [c] Drying rates. [d] Estimated overall heat transfer coefficients.

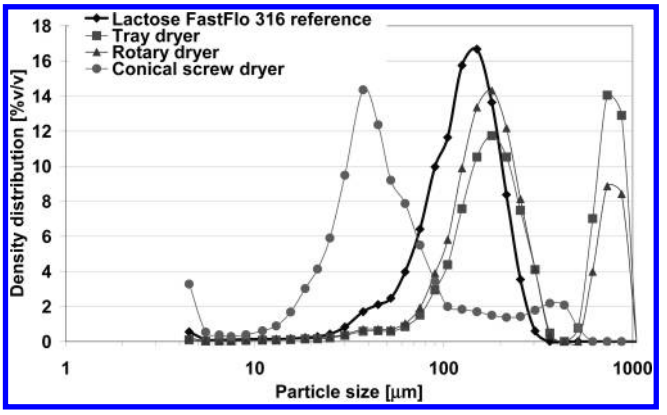

Figure 2. Effect of different laboratory vacuum drying equipment on the particle size distribution of Lactose FastFlo 316 relative to reference.

Case Study 2: Effect of Drying Equipment on Lactose FastFlo 316 and Avicel PH200 Physical Properties. The effect of the drying method on the particle size and size distribution of Lactose FastFlo 316 and Avicel PH200 was evaluated against reference materials. Figure 2 shows the particle size distribution for Lactose FastFlo 316 obtained from tray, rotary, and conical screw drying experimentation compared to reference material. Process conditions used are defined in Table 2.

The median particle size for the reference sample was found to be 116 μm compared to 40, 204, and 205 μm, respectively, for conical screw, rotary dryer, and tray drying experiments. Figure 2 shows that drying performed in the conical screw dryer led to both attrition and agglomeration occurring, as a bimodal PSD is evident. Attrition was found to be the most dominant feature as the median size was reduced from 116 to 40 μm. There was a lower degree of agglomeration evident in the 300−600 μm range. The reduction in particle size is principally due to continuous mechanical agitation with a screw speed of 190 rpm resulting in particle−particle, particle-mixing, and screw and particle-wall collisions. Although the use of mechanical agitation seems to promote an improvement in heat transfer as observed in this study, the effects on the particle size and size distribution can be profound. In contrast, there was no particle attrition associated with tray and rotary drying relative to the reference, and similar median particle sizes were obtained between the drying methods. Similarly, significantly more agglomeration was observed with tray and rotary drying as a bimodal distribution was obtained with agglomerate sizes being significantly larger than conical screw drying. Balling was also observed in the rotary dryer. The frequency of coarse agglomerates in the range of 600−1000 μm was higher with tray drying when compared to rotary drying. This is explained as a result of particles binding together to form larger particles during the drying process.

The Lactose FastFlo 316 drying experiments were repeated using Avicel PH200 instead of using the same drying conditions as defined in Table 2 to assess the impact of laboratory contact vacuum drying on the physical properties. The median particle size for the reference sample was found to be 210 μm compared to 205, 208, and 209 μm respectively for tray dryer, rotary dryer, and conical screw drying experiments. Figure 3 showed that for Avicel PH200 no particle agglomeration was observed with the use of the various drying equipments. Only a marginal decrease in the median particle size was observed due to attrition relative to the reference with each drying method, yielding similar particle size distributions. For Avicel PH200, the impact of using similar drying conditions with various dryers had little influence on the particle size distribution when compared to Lactose FastFlo 316. The observations made in this case are significantly different from

dx.doi.org/10.1021/op1002787 |*Org. Process Res. Dev.* 2011, 15, 360–366

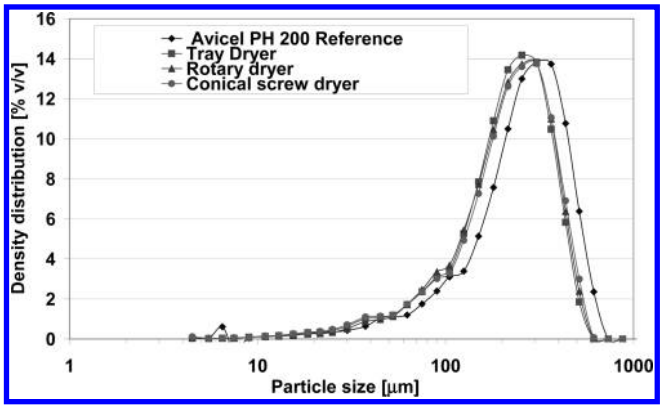

Figure 3. Effect of different laboratory vacuum drying equipment on the particle size distribution of Avicel PH200 relative to reference.

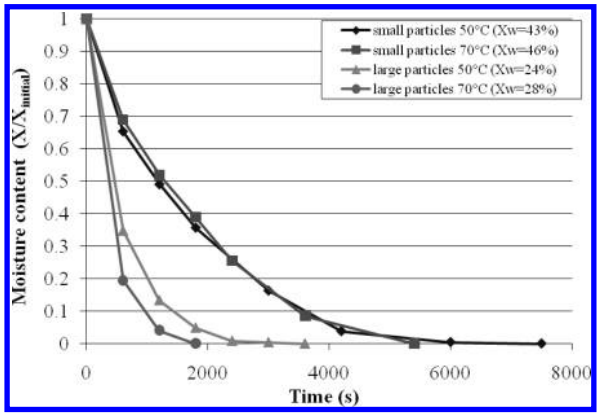

Figure 4. Moisture content versus drying time for the API consisting of 5 and 40 μm median particle sizes [rotary speed = 50 rpm, P = 2 kPa].

those with Lactose FastFlo 316 where a combination of particle attrition and agglomeration was observed. These studies show that material properties influence the impact of drying process conditions on the particle size distribution.

Case Study 3: Active Pharmaceutical Ingredient (API) Drying. Figure 4 shows the variation of moisture content with drying time for median particle sizes of 5 and 40 μm at 50 and 70 °C, respectively, using a constant vacuum level (2 kPa), rotary speed (50 rpm), and batch size (30 g). By increasing the drying temperature from 50 to 70 °C, the overall drying time for particles with a 40 μm median size decreased significantly from 3600 to 1800 s. This confirms observations made in typical industrial drying processes.[18] However, increasing the drying temperature did not have a significant effect on the drying time for particles with a 5 μm median particle size. The rate of removal of moisture content was almost identical during the initial 5500 s of drying. For the small particles being dried at 50 °C, steady-state equilibrium moisture content was not achieved until 7200 s, thus indicating that mass transfer limitations are more evident at lower drying temperatures. Decreasing the median particle size from 40 to 5 μm resulted in an increase in drying time because the initial moisture content is also nearly double postfiltration. This indicates that an increase in median particle size resulted in an increase in deliquoring performance.

Figure 5 shows the effect of rotary speed for particles with a 5 μm median size on the drying time for the API using a constant initial moisture content, drying temperature, and vacuum level.

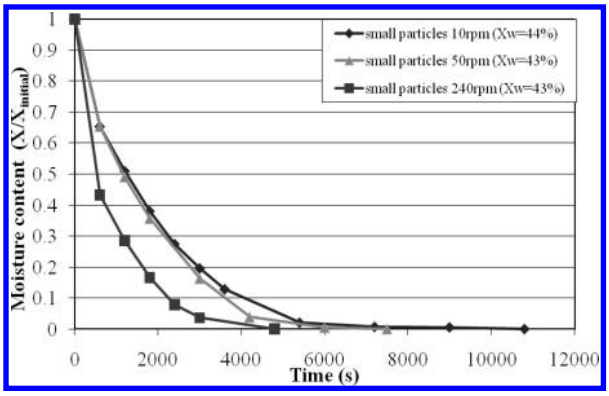

Figure 5. Moisture content versus drying time for the API consisting of 5 μm-sized particles at various rotary speeds [P = 2 kPa, T = 50 °C].

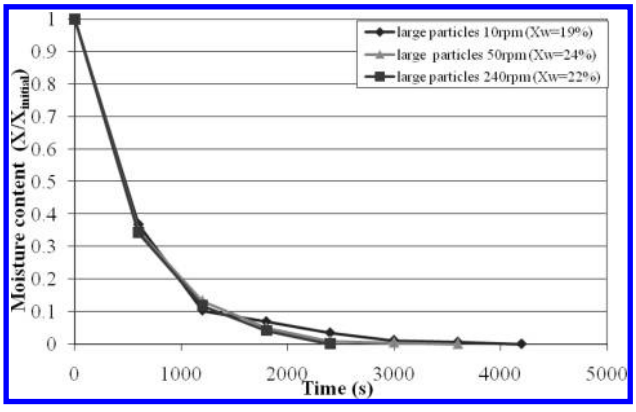

Figure 6. Moisture content versus drying time for the API consisting of 40 μm-sized particles at various rotary speeds [P = 2 kPa, T = 50 °C].

Increasing the rotary speed from 10 to 50 rpm resulted in a small increase in the drying rate and therefore reduction in the overall drying time. However, when the rotary speed was increased to 240 rpm, a significant decrease in the overall drying time was observed with an increase in the drying rate. This is potentially due to the improved efficiency of heat and mass transfer that occurred as a result of increasing the rotary speed including the increased frequency of cake turnover in the drying flask. In contrast, however, increasing the rotary speed from 10 to 240 rpm had little influence on the initial drying rate and drying time (during the initial 2000 s of drying) for particles with a 40 μm median particle size (Figure 6). Increasing the rotary speed reduced the overall drying time and enabled an equilibrium moisture content to be achieved faster. The equilibrium moisture content ranged between 0.1 and 0.2% w/w for all drying experiments.

Figure 7 shows the effect of different vacuum pressures of 2 and 50 kPa to assess the impact on the drying rate on particles with 5 and 40 μm median sizes respectively. A constant rotary speed and drying temperature were used with similar initial moisture contents. Figure 7 shows that reducing the pressure from 50 to 2 kPa had a significant effect on increasing the drying rate and reducing the overall drying time. In the case of using a 40 μm median particle size and although the initial moisture content drying at 2 kPa was 24% w/w compared to 16% w/w at 50 kPa, the drying time was reduced by almost half. The drying rate increased significantly as the pressure was reduced. A lower pressure results in a lowering of the boiling points of solvents. In our

dx.doi.org/10.1021/op1002787 |*Org. Process Res. Dev.* 2011, 15, 360–366

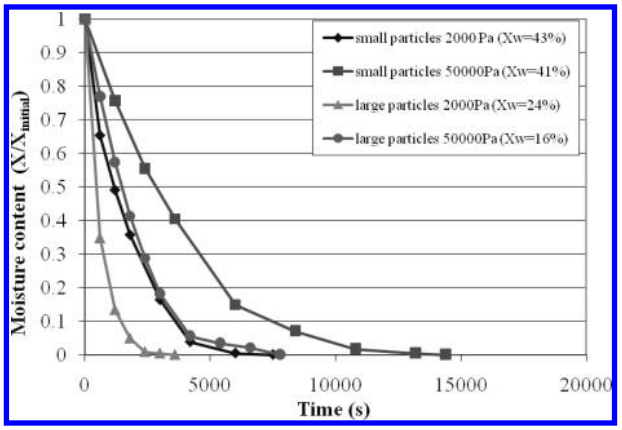

Figure 7. Moisture content versus drying time for the API consisting of 5 and 40 μm median particle sizes at two different vacuum pressures [T = 50 °C, rotary speed = 50 rpm].

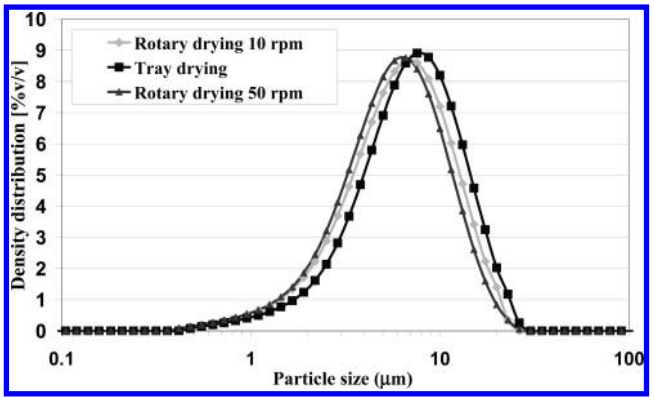

Figure 8. Effect of rotary speed on the particle size reduction of particles with a 5 μm median particle size input compared to the reference input API particle size distribution obtained from tray drying.

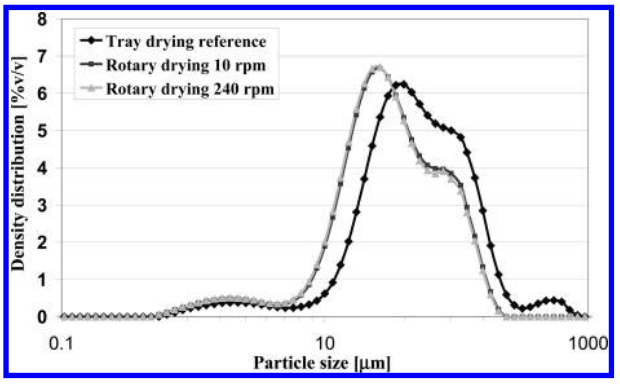

Figure 9. Effect of rotary speed on the particle size reduction of particles with a 40 μm median particle size input compared to the reference input API particle size distribution obtained from tray drying.

case, we assume that the level of acetone post washing with water is negligible. The vacuum pressure in the range of 2−50 kPa corresponds to a water saturation temperature of between 14 and 81 °C. As drying was performed at 50 °C, with a reduced pressure of 2 kPa, the boiling point of water is reduced to 14 °C. This provides a greater temperature difference between medium and product resulting in faster drying.

Figure 8 shows the effect of rotary speed on the particle size of the API obtained from tray drying using a 5 μm median particle size input. A 50 °C drying temperature and 2 kPa vacuum pressure was used in all experiments. An increase in rotary speed from 10 to 50 rpm resulted in further particle size reduction relative to tray drying. With a 40 μm median particle size the effect of rotary drying again resulted in a significant reduction in particle size relative to tray drying. However, an increase in rotary speed from 10 to 240 rpm did not result in any further particle size reduction (Figure 9). Furthermore, the effect of rotary drying resulted in the elimination of coarse agglomerated particles that were observed when tray drying was used.

5. CONCLUSION

The median particle size was found to be a critical parameter when considering the rotary drying of the API. The use of smaller particles resulted in the wet cakes retaining higher initial moisture content, resulting in prolonged drying times when compared to using larger particles. Increasing the rotary speed was found to increase the drying rate and reduce the overall drying time. Furthermore, a reduction in particle size for the API was observed when increasing the rotary speed for both small and large particles. The vacuum level had the most significant impact on the drying time compared to the drying temperature, initial moisture content, and rotary speed. For Lactose FastFlo 316, the laboratory conical screw dryer was found to have the best heat transfer performance due to the effects of improved heat transfer with mechanical agitation. However, the effects of mechanical agitation also resulted in significant attrition and agglomeration of Lactose FastFlo 316. Tray drying was found to have the poorest heat transfer performance and also the largest degree of particle agglomeration when compared to reference material. When considering Avicel PH200, the effect of the various types of laboratory contact vacuum dryers had a minimal impact on the physical properties when compared to the reference material.

This indicates that not only does equipment influence drying performance and the impact on physical properties of materials but also the type of material used itself in a dryer can influence whether agglomeration or attrition would be evident or not.

AUTHOR INFORMATION

Corresponding Author

*Telephone: +44 (0) 1304644374. E-mail: terry.kougoulos@pfizer.com

ACKNOWLEDGMENT

We thank Rachel Yorath and Audrey Morgan for the analytical support relating to particle size determination.

NOMENCLATURE

Q_{bed}	total heat supplied to bed (W)
Q_m	heat used to heat wet material (W)
Q_{ev}	heat used for evaporating the moisture contained in the bed (W)
U	overall heat transfer coefficient (W m^{-2} K^{-1})
A	area available for heat transfer (m^2)
T_m	temperature of the heating medium (K)
T_b	temperature of drying bed (K)

$h_{medium\text{-}walls}$ heat transfer coefficient from heating medium to walls ($W\,m^{-2}\,K^{-1}$)
h_{walls} heat transfer coefficient through the walls ($W\,m^{-2}\,K^{-1}$)
$h_{walls\text{-}particles}$ heat transfer coefficient from inner walls to the first layer of particles ($W\,m^{-2}\,K^{-1}$)
h_{medium} heat transfer coefficient through the bulk material ($W\,m^{-2}\,K^{-1}$)
$h_{medium\text{-}walls}$ heat transfer coefficient for surface evaporation ($W\,m^{-2}\,K^{-1}$)
X/X_i moisture content
X mass of solvent contained in the drying cake (kg)
X_i mass of solvent contained in the wet cake at $t = 0$ min (kg)
W_t mass of drying cake at time t (kg)
LOD cumulative loss on drying (w/w%)
R rate of drying at time t (kg solvent s^{-1} kg $solid^{-1}$)
A area available for heat transfer (m^2)
x_w wall thickness (m)
x_f film thickness (m)

GREEK SYMBOLS

β latent heat of vaporisation of water (J kg_{-}^{1})
λ_G thermal conductivity ($W\,m^{-1}\,K^{-1}$)
λ_V film wall conductivity ($W\,m^{-1}\,K_{-}^{1}$)

REFERENCES

(1) Raha, S.; Kapur, P. *Int. J. Miner. Process.* **2004**, 1–8.
(2) Iritani, E.; Nagaoka, H.; Katagiri, N. *Sep. Purif. Tech.* **2008**, *63*, 379–385.
(3) Docherty, R.; Kougoulos, E.; Horspool, K. *Am. Pharm. Rev.* **2009**, *12*(8), 34−43.
(4) Baker, C. G. J. *Industrial Drying of Food*; Blackie Academic and Professional: London, 1997; Vol. 129, p 188.
(5) Kohout, M.; Collier, A.; Stepanek, F. *Comput.-Aided Chem. Eng.* **2004**, *18*, 1075–1080.
(6) Gevaudan, A.; Andrieu, J. *Chem. Eng. Process.* **1991**, *30*, 31–37.
(7) Michaud, A .; Peczalski, R. J..; Andrieu., J. *Chem. Eng. Process.* **2008**, *47*, 722–730.
(8) Hoektra, L.; Vonk, P.; Hulshof, A. *Org. Process Res. Dev.* **2006**, *10* (3), 409–416.
(9) Toei, R.; Ohmori, T.; Furuta, T.; Okazaki, M. *Chem. Eng. Process.* **1984**, *18*, 149–155.
(10) Colak, N.; Hepbasli, P. *J. Food Eng.* **2007**, *80*, 1188–1193.
(11) Iguaz, A.; Esnoz, A.; Martinez, G.; Lopez, A.; Virseda, P. *J. Food Eng.* **2003**, *59*, 151–160.
(12) Rastikian, K.; Capart, R.; Benchimol, J. *J. Food Eng.* **1999**, *41*, 193–201.
(13) Michaud, A.; Peczalski, R.; Andrieu, J. *Chem. Eng. Res. Des.* **2008**, *86* (6), 606–611.
(14) Forbert, R.; Heimann, F. *Chem. Eng. Process.: Process Intensification* **1989**, *26* (3), 225–235.
(15) Tewari, J.; Dixit, V.; Malik, K. *Sens. Actuators, B* **2010**, *144* (1), 104–111.
(16) Lekhal, A.; Girard, K. P.; Brown, M. A.; Kiang, K.; Glasser, B. J.; Khinast, J. G. *Powder Technol.* **2003**, *132* (2−3), 119–130.
(17) Lekhal, A.; Girard, K. P.; Brown, M. A.; Kiang, K.; Glasser, B. J.; Khinast, J. G. *Int. J. Pharm.* **2004**, *270* (1−2), 263–277.
(18) Mujumbar, A. J. *Handbook of Industrial Drying*; CRC Press: Boca Raton, FL, 2007; pp 114−145.
(19) Rahman, S. *Food Properties Handbook*, 448, FL: CRC Press, 1995.